Effect of increasing disorder on the critical behavior of a Coulomb system

Michael H. Overlin, Lee A. Wong, and Clare C. Yu

Department of Physics and Astronomy, University of California, Irvine, Irvine, California 92697, USA

We have performed a Monte Carlo study of a classical three-dimensional Coulomb system in which we systematically increase the positional disorder. We start from a completely ordered system and gradually transition to a Coulomb glass. The phase transition as a function of temperature is second order for all values of disorder. We use finite size scaling to determine the transition temperature T_C and the critical exponent ν. We find that T_C decreases and that ν increases with increasing disorder. We also observe changes in the specific heat, the single-particle density of states, and the staggered occupation as a function of disorder and temperature.

I. INTRODUCTION

Electrons with long-range Coulomb interactions display a rich and complex behavior. In doped semiconductors and disordered metals, electrons are in the presence of quenched disorder, and the competition between Coulomb interactions and disorder produces a Coulomb glass, which is an amorphous insulator. A great deal of effort has been expended in studying various thermodynamic properties of Coulomb glasses such as the specific heat,[1,2] the presence of a Coulomb glass phase transition in which the electrons are frozen into a highly disordered arrangement[3–7] and the Coulomb gap.[8–10] Coulomb interactions between localized electrons result in the so-called Coulomb gap in the single-particle density of states that is centered at the Fermi energy. Simulations have found a Coulomb gap in the density of states,[3,11–15] and experimental evidence for a Coulomb gap has been seen in tunneling measurements.[16–19]

Many of the theoretical studies of Coulomb glasses have been as a function of temperature. In this paper we will study what happens as we vary the amount of disorder as well as the temperature. We will start with an ordered system and study the effect of gradually introducing disorder into a three-dimensional system of electrons with long-range Coulomb interactions. The system is discrete in the sense that the electrons sit on half of the available sites. In the ordered case the sites form a cubic lattice. The disorder is introduced in the positions of the sites and their deviation from the positions in a cubic lattice. For all values of disorder, the system undergoes a second-order phase transition as the temperature is lowered. We will study the effects on the thermodynamics of this phase transition as a function of disorder.

Discretizing our Coulomb system means that it corresponds to an Ising system with long-range interactions. A site occupied with an electron corresponds to spin up and an empty site corresponds to spin down. This is a very general model, and as a result relevant work has been done in other fields motivated by somewhat different physical systems. In particular, there is the Ising model with long-range interactions. Also the ordered case is related to work that has been done on ionic fluids near criticality. It is worth briefly reviewing the work that has been done in those fields.

In the case of translational invariance, ionic fluids near criticality have been a subject of both experimental and the-

oretical investigations.[20–23] As in the case of electrons, this system is somewhat simplified by discretizing the system and only allowing the charges to sit on specified sites. For ionic fluids this is known as the lattice-restricted primitive model[21–23] (LRPM), where there are equal numbers of positive and negative ions with the same diameter sitting on lattice sites. In the LRPM there is no quenched disorder. There are positive sites, negative sites, and neutral sites (empty sites) corresponding to an Ising spin-1 model with Coulomb interactions. The phase diagram in the density-temperature plane has a second-order transition line from a high-temperature paramagnetic phase to a low-temperature antiferromagnetic phase.[21–23] This transition is in the Ising universality class with critical exponent $\nu = 0.63$. At even lower temperatures there is a first-order phase transition in which the system undergoes a phase separation into a high-density ordered phase and a low-density disordered phase. If there are no neutral sites (ionic density $\rho = 1$), which corresponds to the antiferromagnetic spin-1/2 Ising model, then there is just the second-order transition from the high-temperature disordered phase to the low-temperature ordered antiferromagnetic phase in three dimensions. For the purposes of this article we are interested in this case where there are no neutral sites. Every positively charged site has a positive ion or missing electron, and every negatively charged site has a negative ion or an electron. The fact that the ionic system has a second-order phase transition to an ordered antiferroelectric arrangement of ions[21–23] means that we expect the analogous transition to occur for the case where the electrons can sit on alternate lattice sites with no quenched disorder.

Comparing the ordered and disordered extremes reveals similarities and differences. Both systems undergo a phase transition when the temperature is lowered. In the ordered case, the transition is to an ordered arrangement of electrons occupying every other site, whereas in the disordered case the electrons are frozen into the highly disordered arrangement of a Coulomb glass.[3] Both systems at low temperatures have a gap in their single-particle density of states.

As we mentioned earlier, systems with either positively charged sites (missing electron) or negatively charged sites (electron present) can be mapped onto Ising spin-1/2 systems. A great deal of work has been done on Ising models with long-range interactions. The ferromagnetic or attractive

Ising model with power law interactions that fall off as $1/r^\eta$ without quenched disorder has been studied[24,25] as a function of the dimension d and the exponent η for $\eta \geq d$. However, in this paper we will focus on interacting electrons and so we are interested in the antiferromagnetic Ising model.

The presence of quenched disorder results in an Ising spin glass. There has been a substantial amount of numerical effort to understand the energy of domain walls at $T=0$.[26–33] The energy of the domain wall varies as L^θ, where L is the system size and the exponent θ is positive for systems with nonzero transition temperatures. Work on the Ising spin glass with power law interactions has been summarized in a couple of papers.[26,34] The system has a rich phase diagram in the d-η plane, which can be found in Ref. 26, where d is the dimension and η is the exponent of the power law interaction $1/r^\eta$. The smaller the η, the longer the range of the interaction. If the range is long enough or if the dimension is large enough, then there is a second-order phase transition with a transition temperature $T_C > 0$. The critical exponents are different in the long-range and short-range regimes. The exponent θ depends continuously on η in the long-range region ($\theta = d - \eta$), and is independent of η in the short-range regime.[26] This indicates that the critical exponents also depend continuously on η in the long-range region, and are independent of η in the short-range regime.[26] Katzgraber and Young have done Monte Carlo simulations of an Ising spin glass in one dimension with long-range interactions.[26,27] They chose a value for η where the system has a second-order spin glass transition, and they find that $\nu = 10/3$.

In this paper we will be concerned with what happens to thermodynamic quantities as we systematically introduce disorder into a three-dimensional system of electrons with long-range Coulomb interactions. The disorder is introduced into the placement of sites where the electrons can sit. The paper is organized as follows. In Sec. II we present the Hamiltonian and describe our Monte Carlo simulation. In Sec. III we present the quantities that we measure. In Sec. IV we present our results, and we give our conclusions in sec. V.

II. CALCULATION

A. Hamiltonian

Let us start by considering the completely disordered case, which is known as a Coulomb glass. The essential physics of the Coulomb glass is the presence of both disorder and long-range Coulomb interactions between electrons. The Hamiltonian often studied for the Coulomb glass is[4,35]

$$H = \sum_i n_i \phi_i + \sum_{i>j} \frac{(n_i - K)(n_j - K)}{r_{ij}}, \qquad (1)$$

where we set the charge $e=1$, $n_i = \pm 1$ is the number operator for site i, ϕ_i is the on-site energy, $r_{ij} = |\vec{r}_i - \vec{r}_j|$, and K is a compensating background charge making the whole system charge neutral. Such a Hamiltonian describes a lightly doped semiconductor, in which the impurity sites are far enough apart that the overlap between sites can be neglected. In most of the early work on the Coulomb glass (e.g., Refs. 4, 6, and 35), the sites are chosen to form a periodic lattice, and the

disorder is present in the form of random on-site energies. For an ordered system, the on-site energy ϕ_i is a constant. One could imagine gradually introducing disorder by allowing ϕ_i to be chosen from a distribution whose width gradually increases.

However, the presence of random on-site energies makes numerical analysis difficult, since even in the high-temperature state the average occupation of a site is not zero. This makes the search for a phase transition difficult; there is no obvious order parameter that becomes nonzero at the transition. For our numerical analysis, it is more convenient to take the disorder to be entirely in the location of the sites. This changes the symmetry of the Hamiltonian from having on-site disorder to having disorder in the interaction between sites because the distance between sites varies. For many quantities these two models give similar results. For example, studies of the specific heat in Coulomb glasses have compared having disorder in the on-site energy to having a completely random displacement of sites.[2,36] They find that both models produce qualitatively similar results with some quantitative differences. However, the existence and nature of the phase transitions are different in the two models.[37,38] In particular, there is always a phase transition no matter how wide the distribution of the site placement is, whereas there is no phase transition if the width of the distribution of the on-site energy ϕ_i is larger than a critical value.[39] Möbius[39] has argued that such a critical value must exist, even if it is vanishingly small, since there is a phase transition when there is no disorder[40] while there is no clear evidence for a transition when there is substantial on-site disorder. This implies that long-range order is destroyed by both on-site disorder and thermal fluctuations.

A number of previous simulations have used the form for the Hamiltonian with disorder in the placement of the sites.[2,3,36,41] In the case of half filling there is a particle-hole symmetry, and the phase transition is associated with the development of a nonzero Edwards-Anderson order parameter.[3] We therefore rewrite the Hamiltonian (taking $K = 1/2$) to look like that of a spin glass,

$$H = \frac{1}{4} \sum_{i>j} \frac{S_i S_j}{r_{ij}}. \qquad (2)$$

$S_i = 1(-1)$ will denote an occupied (unoccupied) site.

We have simulated three-dimensional systems of linear size $L = 4$, 6, and 8. We place $N = L^3$ sites in the system. We have only considered the case of half filling in order to take advantage of the spin-flip symmetry. For the ordered case the sites form a cubic lattice. In the ground state, every other site is occupied; the occupied sites form a face-centered-cubic (fcc) lattice. We can gradually introduce disorder by allowing the deviation of a site from its position in a cubic lattice to be chosen from a Gaussian distribution with a standard deviation of σ. This gives the radial distance from the cubic lattice site. The angular coordinates of the site are chosen randomly using a uniform distribution. The ordered case corresponds to $\sigma = 0$. $\sigma = 1$ corresponds to the very disordered case with a standard deviation equal to the cubic lattice constant a. We also considered completely random arrangements of sites

where the x, y, and z coordinates of each are chosen from a uniform distribution. We call this the "uniform random" case. We find no qualitative difference and only a slight quantitative difference between the uniform random case and the $\sigma=1$ case in quantities such as the single-particle density of states, the specific heat versus temperature, and Binder's g. So we will not make much mention of the uniform random case.

We use infinite periodic boundary conditions in which the simulation box is infinitely replicated in all directions to form a lattice. As a result, an electron on a given site interacts with other electrons and all their images via the Coulomb interaction. To handle this, we use an Ewald summation technique[42] that replaces the Hamiltonian in Eq. (2) with the following effective interaction between sites:

$$H = \sum_{1 \le i < j \le N} \frac{1}{L} q_i q_j \psi\left(\frac{\vec{r}_{ij}}{L}\right) + \frac{\Lambda}{2L} \sum_{i=1}^{N} q_i^2, \tag{3}$$

where L is the linear size of the simulation box, N is the number of sites, the charge $q_i = S_i/2$, and the function $\psi(\vec{r})$ is given by

$$\psi(\vec{r}) = \sum_n \frac{\text{erfc}(\alpha|\vec{r}+\vec{n}|)}{|\vec{r}+\vec{n}|} + \frac{1}{\pi} \sum_{n \ne 0} \frac{1}{|\vec{n}|^2} \exp\left\{ 2\pi i \vec{n} \cdot \vec{r} - \frac{\pi^2 |\vec{n}|^2}{\alpha^2} \right\} \tag{4}$$

in which

$$\text{erfc}(x) = 1 - \frac{2}{\sqrt{\pi}} \int_0^x e^{-t^2} dt \tag{5}$$

is the complementary error function and

$$\Lambda = \sum_{\vec{n} \ne 0} \left[\frac{\text{erfc}(\alpha|\vec{n}|)}{|\vec{n}|} + \frac{1}{\pi|\vec{n}|^2} e^{-\pi^2 n^2/\alpha^2} \right] - \frac{2\alpha}{\sqrt{\pi}}. \tag{6}$$

Note that

$$\Lambda = \lim_{|r| \to 0} \left[\psi(\vec{r}) - \frac{1}{|\vec{r}|} \right]. \tag{7}$$

The sum over $\vec{n}$ in Eq. (6) is a sum over all simple-cubic lattice points with integer coordinates $\vec{n}=(l,m,n)$. These are the coordinates of the images of the simulation box. The parameter α is a convergence factor that is adjusted to maximize the rate of convergence of the sum. We have omitted a positive term in the Hamiltonian (3) that is proportional to the square of the net dipole moment of the configuration.[42] This omission is equivalent to the boundary condition in which the infinite sphere of our system and its images are surrounded by a perfect conducting medium. We have done some runs with the dipole term and find no qualitative difference and only a slight quantitative difference compared to the case with no dipole term. So in this paper we will present the result of simulation runs that omit the dipole term.

B. Monte Carlo simulation

We have used a Monte Carlo heat bath algorithm. We keep a table of the potential energy at each site. Each electron is looked at sequentially and moved to one of the available $N/2+1$ sites (its own site or one of the available $N/2$ unoccupied sites), chosen with a Boltzmann probability. If the site chosen is the electron's original location, the potential energies are unchanged; if the electron hops to a new site, we update all the potential energies. If the electron chooses its initial site, which it does with high probability at low temperatures, we do not have to recompute the potential energies. This speeds up the simulation considerably, partially compensating for the much longer equilibration times needed at low temperatures. Our longest run (for $L=4$ at $T=0.01$ and $\sigma=0.5$) had 3×10^6 Monte Carlo steps per electron. Depending on the system size and temperature, the sample averages involved between 5 and 190 disorder configurations.

III. MEASURED QUANTITIES

A. Binder's g and equilibration criteria

The Edwards-Anderson order parameter alluded to above quantifies the extent to which spins or site occupations are frozen. It is defined as $q \equiv [\langle S_i \rangle^2]$; we will denote thermal averages by $\langle \cdots \rangle$ and disorder averages by $[\cdots]$. Thermal averages sum over fluctuations in the positions of the electrons weighted with the correct Boltzmann probability; disorder averages sum over different arrangements of the sites. We can see from the definition of q that if the spins are frozen, then the average orientation of a spin will have a nonzero thermal average and q will be finite. This is why q can be thought of as the order parameter of the phase transition.

We can generalize the Edwards-Anderson order parameter to a finite time overlap in either of two ways.[43] The first way computes the overlap between two replicas:

$$q_r(t) = \frac{1}{N} \sum_i S_i^{(1)}(t) S_i^{(2)}(t), \tag{8}$$

where the superscripts refer to different replicas. The two replicas are identical in their disorder, i.e., the placement of the sites, but differ in the initial positions of the electrons. The other way uses the same replica at two different times:

$$q_t(t,\tau) = \frac{1}{N} \sum_i S_i^{(1)}(t) S_i^{(1)}(t+\tau). \tag{9}$$

If the time difference τ is sufficiently large that the electron configurations at t and $t+\tau$ are essentially uncorrelated, $q_t(t,\tau)$ will give the same result as the replica overlap.

We use the moments of the overlap to define Binder's g, which is a parameter that is related to the phase transition. First we define $g(\tau)$ by[43,44]

$$g(\tau) = \frac{1}{2}\left(3 - \frac{[\langle q^4(\tau) \rangle]}{[\langle q^2(\tau) \rangle]^2} \right), \tag{10}$$

where

$$\langle q^n(\tau) \rangle = \frac{1}{\tau} \sum_{t=\tau}^{2\tau} q^n(t). \tag{11}$$

We will use g_t (g_r) to denote the result of using q_t (q_r). Binder's g is given by

$$g = \lim_{\tau \to \infty} g(\tau), \tag{12}$$

which we will approximate by

$$g \approx g(\tau) \tag{13}$$

for some measurement time τ large enough that the configurations are essentially uncorrelated so that g_t and g_r agree. We have used this fact to monitor equilibration by simulating two replicas that have the same placement of sites but different spin configurations.[43] Typically $g_r(t)$ increases with time to the equilibrium value, whereas $g_t(t)$ decreases to the equilibrium value. The two methods agree when the system has reached equilibrium. Our criterion for equilibration was that the values of g_r and g_t agreed to within 0.1. We only present results for systems that meet this criterion. We should caution that this criterion can be met even though the system may still be slowly aging.

Binder's g provides a way to monitor the phase transition. At high temperatures, the distribution of q tends to a Gaussian so that $g \to 0$, whereas the order parameter, and hence g, become nonzero as the temperature approaches the phase transition temperature T_C. If we make the assumption of one parameter scaling, then the only relevant length is the correlation length $\xi \sim (T - T_C)^{-\nu}$, where ν is the critical exponent associated with ξ. So all lengths, including L, can be scaled by ξ. Since g is dimensionless, we expect that it should satisfy a scaling form[43,44]

$$g(L,T) = \hat{g}(L^{1/\nu}(T - T_C)). \tag{14}$$

Thus at the critical temperature, $g(L, T_C)$ should have the same value independent of the system size L (as long as L is sufficiently large for finite size scaling to apply).[43,44]

B. Specific heat

There are two ways to calculate the specific heat $C_V(T)$. The first way uses the variance of the energy fluctuations:

$$C_V = \frac{1}{Nk_B T^2}[\langle E^2 \rangle - \langle E \rangle^2], \tag{15}$$

where E is the average energy per electron, N is the number of electrons, and k_B is Boltzmann's constant. The other way to calculate the specific heat is to take the derivative of the energy with respect to temperature. We can approximate the derivative by a finite temperature difference

$$C_V(T_i) = \left. \frac{\partial [\langle E \rangle]}{\partial T} \right|_{T_i} \approx \frac{[\langle E(T_{i+1}) \rangle] - [\langle E(T_i) \rangle]}{(T_{i+1} - T_i)}. \tag{16}$$

We found that the specific heat calculated in these two ways agreed quite well. Notice however, that if the slope of E versus T is increasing as temperature increases, then the spe-

cific heat calculated by the finite difference method will underestimate C_V, which is actually the slope of the tangent to the energy curve. Similarly, if the slope of E versus T is decreasing as the temperature increases, the finite-difference method will overestimate C_V.

C. Staggered occupation

Since an unoccupied site on a cubic lattice corresponds to a down Ising spin and an occupied site to an up Ising spin, the fcc crystalline phase corresponds to a maximum in the magnitude of the staggered occupation M_s. The staggered occupation is defined by[7]

$$M_s = \frac{1}{N} \sum_i (-1)^{i+j+k} S_{i+j+k}, \tag{17}$$

where i, j, k are the integer coordinates of the sites in a cubic lattice in units of the lattice constant a. So a site coordinate $(x, y, z) = (ia, ja, ka)$. Since disorder is introduced through a distribution in the position of the sites with respect to the cubic lattice sites, we can still use Eq. (17) to calculate the staggered occupation in the presence of disorder by regarding i, j, and k as coordinates of the center of the unit cell where the site is located. It is useful to plot the staggered occupation distribution $P(M_s)$ versus M_s in order to see the extent of the "crystalline" order. In order to compare different system sizes, we normalize the staggered occupation to range from -1 to $+1$, and the area under the curve is normalized to 1.

D. Single-particle density of states

We have calculated the single-particle density of states $N(E)$ at various temperatures. $N(E)$ is the distribution of potential energies at single sites due to interactions with all the other sites. In other words, we can write the Hamiltonian in the form of an Ising model:

$$H = -\frac{1}{2} \sum_{ij} J_{ij} S_i S_j = \sum_i E_i S_i, \tag{18}$$

where E_i is the single-site energy or "local field" and is given by

$$E_i = -\frac{1}{2} \sum_j J_{ij} S_j. \tag{19}$$

$N(E)$ is the thermally averaged and disorder-averaged distribution of E_i.

IV. RESULTS

A. Second-order melting transition in the ordered case ($\sigma = 0$)

We consider the case where the translational degrees of freedom are discrete and the electrons can only sit on designated sites. This is equivalent to a long-range Ising model in three dimensions. If the sites are ordered and are lattice sites, it is also equivalent to the LRPM in the completely filled case (ionic density $\rho = 1$).[23] We find that discretization pro-
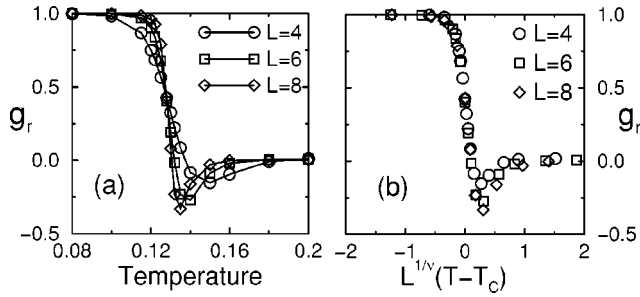
FIG. 1. (a) $g_r(L,T)$ vs T for $\sigma=0$. [$g_t(L,T)$ vs T is virtually identical.] The data for $L=4$ are averaged over 190 runs, $L=6$ is averaged over 67 runs, and $L=8$ is averaged over 45 runs. The solid lines are guides to the eye. (b) $g(L,T)$ for $\sigma=0$ scaled using $\hat{g}(L^{1/\nu}(T-T_C))$ with $T_C=0.128\pm0.001$ and $\nu=0.55\pm0.1$.

FIG. 2. The distribution $P(M_S)$ of the staggered occupation M_S for $L=8$ at $\sigma=0$ at various temperatures. The central peak is highest at $T=1$ and gradually decreases as T decreases. The two side peaks begin to appear in the vicinity of T_C and become more pronounced as T drops below T_C. There is no temperature where three peaks are present, indicating that the transition is not first order. The data were the result of averaging over 35 runs.

duces a second-order phase transition regardless of the amount of positional disorder. In this section we present evidence that the ordered case with $\sigma=0$ undergoes a second-order crystallization transition to an fcc lattice as the temperature is lowered. This result is consistent with the second order transition found by Möbius and Rößler[40] from numerical simulations of a half-filled system on a cubic lattice with Coulomb interactions. It is also consistent with the second-order transition in the LRPM model for the fully occupied case ($\rho=1$).[23,45]

In Fig. 1 we show g versus the temperature T at $L=4$, 6, and 8. The point where these curves cross yields a transition temperature of $T_C=0.127$. Notice that above the transition g dips down and acquires negative values. This behavior has been seen in the case of a three-state ferromagnetic Potts model in three dimensions that undergoes a first-order phase transition.[46] However, in that case the value of g at the minimum scaled as $g(T_{\min})\sim-L^d$, whereas in our case $g(T_{\min})$ appears to saturate at large L. The negative values of g can result if the distribution $P(q)$ is non-Gaussian with finite weight at $q\neq0$ corresponding to long lived occupations of some sites. A very simple δ-function distribution that illustrates this is

$$P(q) = \alpha_0\delta(q) + \left[\frac{1-\alpha_0}{2}\right]\delta(q-a_0) + \left[\frac{1-\alpha_0}{2}\right]\delta(q+a_0),$$
$$(20)$$

where α_0 is a parameter with values between 0 and 1, and a_0 is a constant. For $2/3<\alpha_0<1$, this distribution yields $g<0$.

We initially thought that the transition might be first order. One of the signatures of a first-order melting transition is the coexistence of the liquid and crystalline phases at the melting temperature. We looked for evidence of coexistence by examining the distribution $P(M_s)$ of the staggered occupation. Coexistence would produce three peaks in $P(M_s)$ versus M_s: a central peak and two side peaks symmetrically placed with respect to $M_s=0$. The central peak corresponds to the high-temperature liquid phase and the side peaks correspond to the fcc crystalline phase. Furthermore, at the transition temperature for a first-order transition, the three peaks would
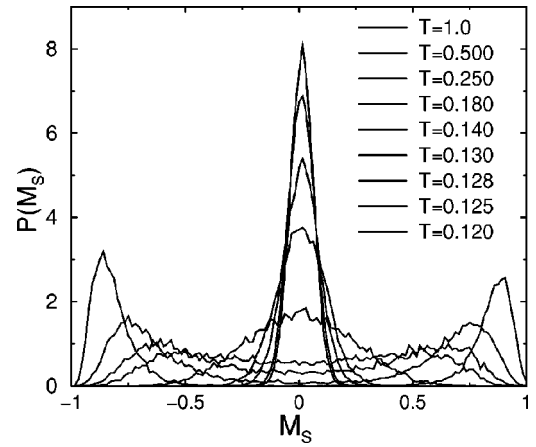
become narrower and higher with increasing system size. On the other hand, if the system is cooled through a second-order transition, the high-temperature central peak in $P(M_s)$ is replaced by two peaks symmetrically placed about $M_s=0$. These peaks do not become sharper with increasing system size, but the width of the distribution is expected to decrease with increasing system size as $L^{-\beta/\nu}$, where β and ν are the critical exponents defined by $M_s\sim|T-T_C|^\beta$ and $\xi\sim(T-T_C)^{-\nu}$.[47]

Figure 2 shows the distribution $P(M_s)$ of the staggered occupation at various temperatures. Notice that in the vicinity of the melting temperature there are only two symmetrical side peaks. This implies that the transition is a second-order phase transition. Furthermore we find that the value $M_{s,max}$, where $P(M_s)$ has a maximum, decreases with increasing system size at T_C and varies as $M_{s,max}\sim L^{-0.6}$. This is also consistent with a second-order transition. In the vicinity of the phase transition where $P(M_s)$ has two peaks, we can define the width $M_{s,width}$ of the distribution as the nonzero value of M_s where $P(M_{s,width})=P(M_s=0)$. We find at T_C that $M_{s,width}$ is linear in L and can be fitted to the form $M_{s,width}=A-mL$, where A and m are constants that are temperature dependent. At $T=0.128$, which is close to T_C, $A=1.1$, and $m=0.027$. Notice that $M_{s,width}$ does not appear to follow the form $M_{s,width}\sim L^{-\beta/\nu}$, but we would need more than three values of L to accurately determine if there is a discrepancy with the scaling form.

First-order phase transitions are often characterized by hysteresis upon heating and cooling. We have looked for hysteresis by cooling and then heating the system, and examining the resulting curves of g versus T as well as the specific heat C_V versus T. We find no hysteresis, which is further evidence against a first order phase transition. To summarize, the ordered case ($\sigma=0$) undergoes a second-order phase transition as a function of temperature.
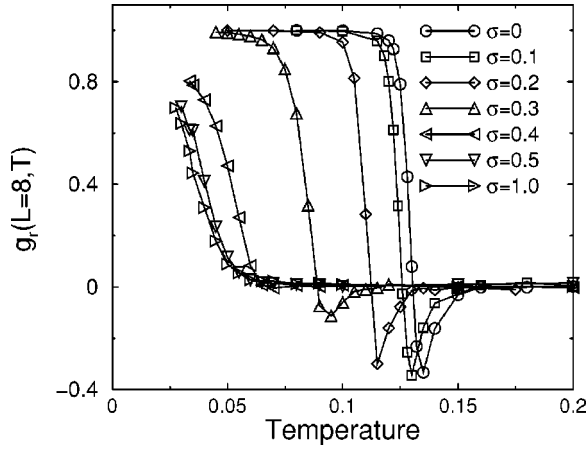
FIG. 3. $g_r(L=8,T)$ vs T for $\sigma=0$ (45 runs), $\sigma=0.1$ (10 runs), $\sigma=0.2$ (5 runs), $\sigma=0.3$ (15 runs), $\sigma=0.4$ (115 runs), $\sigma=0.5$ (45 runs), and $\sigma=1$ (108 runs). [$g_t(L=8,T)$ vs T is virtually identical.] The number of runs in parentheses is the number of runs that were averaged to obtain the data. The solid lines are guides to the eye.

B. Critical behavior

We have determined the critical exponent ν and the transition temperature T_C as a function of the disorder σ through the finite size scaling of $g(L,T)$.[3,43] In Fig. 3 we plot $g(L=8,T)$ versus T for various values of σ. Notice that the transition region moves to lower temperatures with increasing disorder. This reflects the decrease in T_C with increasing σ. The transition temperature corresponds to the temperature where the curves of $g(L,T)$ versus T for all sizes cross. Examples are shown in Figs. 1 and 4.

To more accurately determine T_C, we use the scaling hypothesis to collapse the data for a given value of σ onto a single curve as shown in Fig. 4. T_C and ν are used as adjustable parameters to collapse the data. The values of ν and T_C at various values of σ are given in Table I. We can estimate the errors in the critical temperature and the critical exponent ν by how well the curves can be made to collapse. The errors given in the table also include our estimate of the effects of aging. In other words, the error bars include our estimate of how the values might change if we were to run longer at low temperatures or cool more slowly. In Figures 5 and 6 we plot T_C and ν versus σ.

We can see that ν increases from $\nu=0.55\pm0.1$ at $\sigma=0$ to $\nu=1.30\pm0.2$ at $\sigma=1$. The value of ν in the ordered case ($\sigma=0$) lies between the classical value ($\nu=0.5$) and the value for the ordered short-ranged Ising model ($\nu=0.63$).[48] Within the error bars, our value is consistent with both universality classes, and we therefore cannot differentiate between them. Möbius and Rößler[40] studied a half-filled system on a cubic lattice with Coulomb interactions and found $\nu=0.635(10)$, which agrees with the value for the Ising model. Our simulations differ from those of Möbius and Rößler in that we used the Ewald summation to take into account the fact that the Coulomb interaction extends beyond the size of the system while they did not. As we mentioned earlier, the order-disorder transition in the LRPM model on a simple-cubic lattice belongs to the Ising universality class.[45]
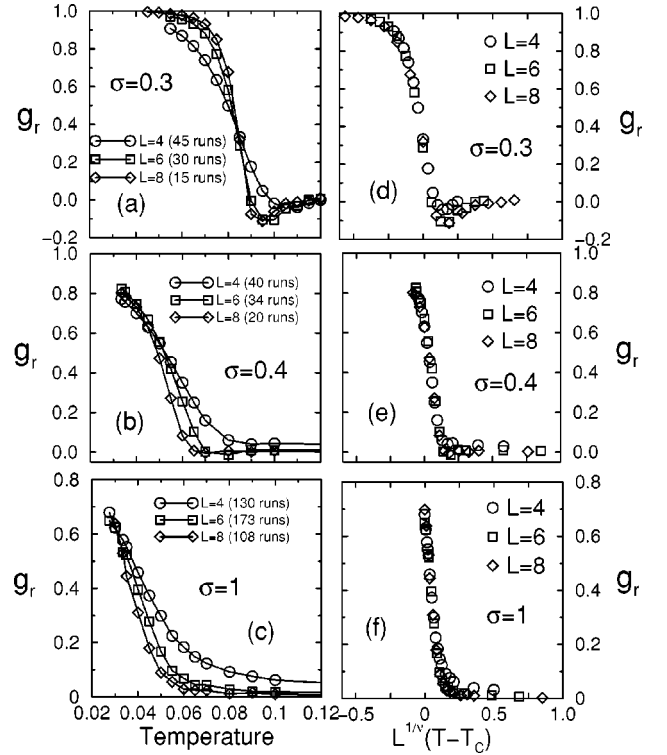

FIG. 4. (a)-(c) $g_r(L,T)$ vs T for $\sigma=0.3$, 0.4, and 1.0 at $L=4$, 6, and 8. The solid lines are guides to the eye. [$g_t(L,T)$ vs T is virtually identical.] The number of runs in parentheses is the number of runs that were averaged to obtain the data. (d) $g_r(L,T)$ for $\sigma=0.3$ scaled using $\hat{g}(L^{1/\nu}(T-T_C))$ with $T_C=0.085\pm0.005$ and $\nu=0.71\pm0.1$. (e) $g_r(L,T)$ for $\sigma=0.4$ scaled using $\hat{g}(L^{1/\nu}(T-T_C))$ with $T_C=0.045\pm0.01$ and $\nu=1.05\pm0.1$. (f) $g_r(L,T)$ for $\sigma=1$ scaled using $\hat{g}(L^{1/\nu}(T-T_C))$ with $T_C=0.028\pm0.01$ and $\nu=1.30\pm0.2$.

The completely filled LRPM model with ionic density $\rho=1$ is equivalent to our $\sigma=0$ case. In addition, Luijten *et al.* did Monte Carlo studies of the restricted primitive model (RPM), which has equal numbers of oppositely charged ions with equal diameters and with Coulomb interactions in three dimensions.[49] These grand canonical simulations of the RPM used a finely discretized lattice where the ionic diameters were 5 times larger than the lattice spacing, and they found the Ising of the critical exponent $\nu=0.63(3)$.

In the disordered case ($\sigma=1$) our value for $\nu=1.3\pm0.2$ differs from the value of $\nu=0.75^{+0.2}_{-0.1}$ obtained earlier.[3] Again this is probably due to the fact that we used Ewald summa-

TABLE I. The values of T_C and ν for different valuse of σ.

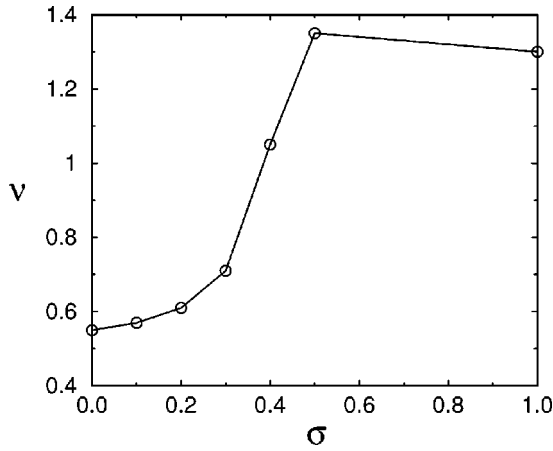| σ	T_C	ν
0.0	0.128±0.005	0.55±0.1
0.1	0.123±0.005	0.57±0.1
0.2	0.110±0.005	0.61±0.1
0.3	0.085±0.005	0.71±0.1
0.4	0.045±0.01	1.05±0.2
0.5	0.030±0.01	1.35±0.2
1.0	0.028±0.01	1.30±0.2

FIG. 5. The critical exponent ν vs the disorder σ. The solid line is a guide to the eye.

tion whereas the previous work did not. In addition we were able to do longer runs at low temperatures than the previous work.

The transition temperature decreases from T_C =0.128±0.005 at σ=0 to T_C=0.028±0.01 at σ=1. The value of T_C=0.128 at σ=0 is consistent with the temperature of the peak in the specific heat found previously by Möbius and Rößler.[40] Within the error the value of T_C=0.028±0.01 at σ=1 is consistent with the previous value of T_C =$0.043^{+0.003}_{-0.006}$ found by Grannan and Yu.[3]

It is interesting that T_C is much lower than the characteristic energies of the system which are of order unity. This is especially true for large values of the disorder. The reason for this was given by Grannan and Yu[3] and is as follows. At the temperatures of our simulations, nearby pairs of sites will with high probability consist of an occupied and an unoccupied site. Since these strongly coupled pairs of sites are close together, they are guaranteed to have small dipole moments. Therefore, they will interact weakly with the rest of the system, remaining active down to temperatures much lower than the bare interaction energy.
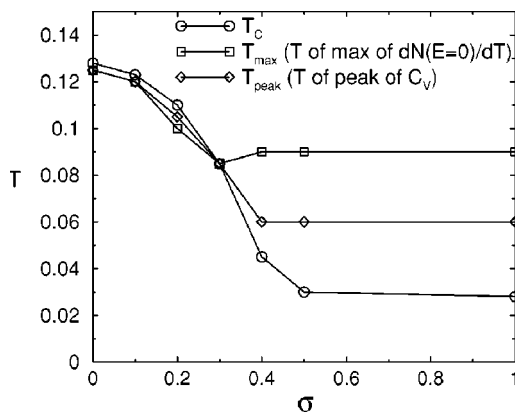
FIG. 6. Transition temperature T_C vs σ (◯), temperature T_{max} of the maximum of $dN(E=0)/dT$ vs σ (□), and the temperature T_{peak} of the maximum in the specific heat vs σ (◇). The solid lines are guides to the eye.
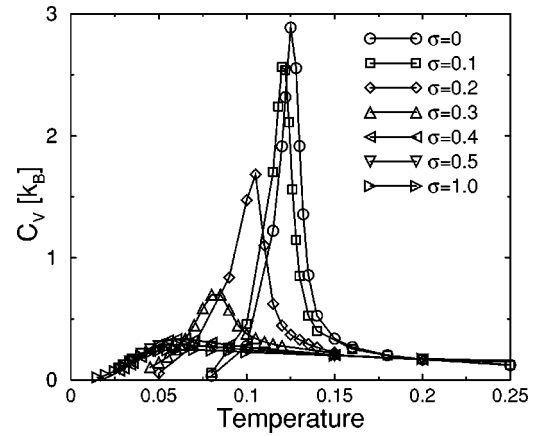

FIG. 7. The specific heat C_V vs T in units of k_B for L=8 for σ =0 (45 runs), σ=0.1 (10 runs), σ=0.2 (5 runs), σ=0.3 (15 runs), σ=0.4 (95 runs), σ=0.5 (45 runs), and σ=1 (108 runs). The number of runs averaged over is indicated in parentheses. The solid lines are guides to the eye.

C. Specific heat

In Fig. 7 we plot the specific heat versus temperature for various values of σ for L=8. We see that in the ordered case (σ=0) C_V exhibits a sharp peak centered at T_C. As the disorder increases, the peak broadens and eventually becomes a broad bump with a maximum at a temperature above T_C. For example, for σ=1, C_V has a maximum at T=0.07, whereas T_C=0.028. In Fig. 6 we compare the temperature T_{peak} of the maximum in the specific heat with T_C for various values of σ. We see that T_{peak} matches well with T_C for $\sigma \lesssim 0.3$. For larger values of σ, $T_{peak}>T_C$. Spin glasses also have a maximum in their specific heat at a temperature above the spin glass transition temperature.[50] For the three-dimensional Coulomb glass where the disorder is in the on-site energy rather than in the positions of the sites, Möbius et $al.$ found that as the width in the distribution of on-site energies increased, the temperature T_{peak} of the maximum in the C_V also increased.[1,2] However, in the cases of on-site disorder that they considered, the maximum does not signify a transition since the existence of a phase transition in the presence of on-site disorder has not been established. The maximum in C_V must be present since $C_V(T)$ goes to zero at the extremes $T \rightarrow 0$ and $T \rightarrow \infty$, implying that there must be a maximum between these extremes.[39] Furthermore, even without Coulomb interactions but with a large amount of on-site disorder, there would be a maximum in the specific heat consisting of a superposition of the Schottky specific heats of two-level systems with randomly distributed excitation energies.[39]

To show the size dependence of the specific heat, in Fig. 8 we plot C_V versus T for different system sizes at σ=0 and at σ=1. In the ordered case the specific heat peak becomes sharper as L increases, while in the disordered case, the broad bump is only weakly dependent on system size.

D. Single-particle density of states $N(E)$

In a Coulomb glass the long-range Coulomb interactions between localized electrons produce a Coulomb gap in the
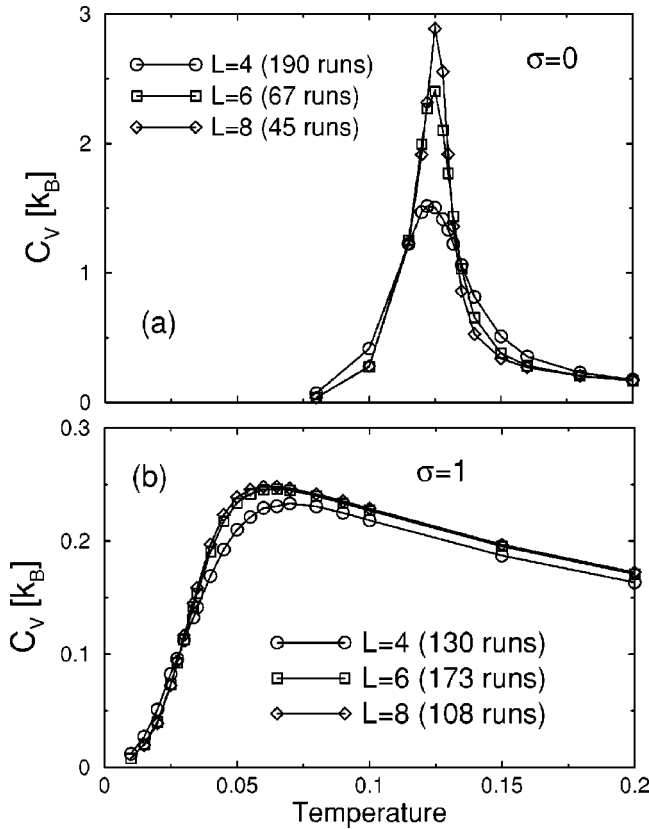
FIG. 8. The specific heat C_V vs T in units of k_B for $L=4$, 6, and 8 for (a) $\sigma=0$ and (b) $\sigma=1$. The specific heat is calculated from the variance in the energy fluctuations. The specific heat calculated from the derivative of the energy with respect to temperature is similar. The number of runs averaged over is indicated in parentheses. The solid lines are guides to the eye.

FIG. 9. $N(E)$ versus E for $L=8$ at various temperatures. The solid lines are guides to the eye. (a) $\sigma=0$. The data were averaged over 45 runs. (b) $\sigma=1$. The three lowest temperatures were averaged over 108 runs and the three highest temperatures were averaged over 16 runs.

single-particle density of states that is centered at the Fermi energy.[8–10] The Coulomb gap makes the ground state stable with respect to single-electron hops. The ordered case also has a gap but for a somewhat different reason. In the ground state of the ordered case where there is a fcc lattice, the potential energy or local field is the same for each occupied site. The local field is equal and opposite for the unoccupied sites. This leads to an $N(E)$ with two δ functions symmetrically placed about $E=0$. In finite size systems at finite temperatures these δ functions broaden into finite height peaks due to thermal fluctuations and the formation of ordered domains.

In Fig. 9 we show the density of states $N(E)$ for single-particle excitations at various temperatures for $\sigma=0$ and for $\sigma=1$. Because of strong electron-electron correlations, the density of states at zero energy starts to decrease at about $2T_C$ in the ordered case ($\sigma=0$) but at a temperature about an order of magnitude above T_C in the strongly disordered case ($\sigma=1$). In Fig. 10 we show $N(E)$ at or near T_C for various values of σ for $L=8$. We see that at T_C the gap appears nearly fully formed for $\sigma=1$ but not for $\sigma=0$. In the ordered case the finite density of states at $E=0$ is possibly due to domains.

As we can see from the figures, at finite temperatures the gap in the density of states is partially filled, and the density
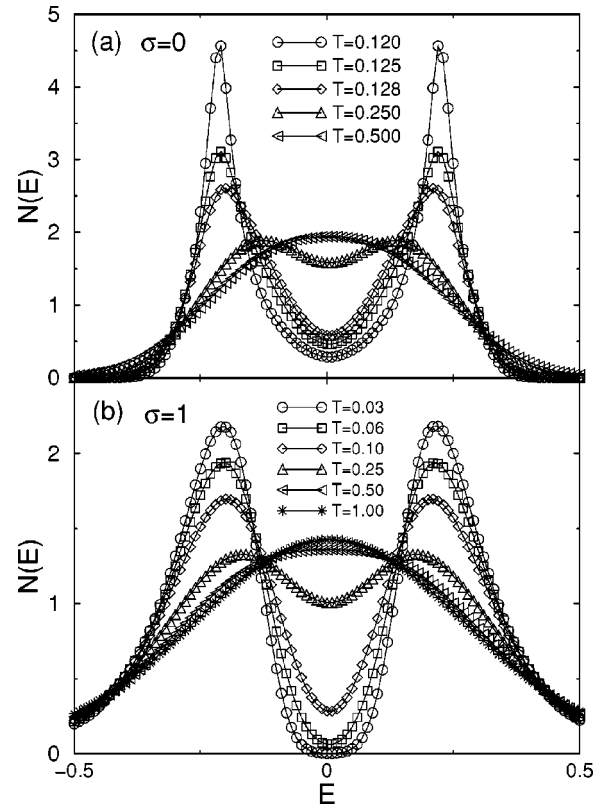
of states does not vanish at the Fermi energy. This has been seen in previous simulations.[3,11–15] Tunneling measurements of the Coulomb gap have also seen that it fills in with increasing temperature.[18,19] The exact form of $N(E,T)$ is not known, but for strong disorder some have argued[11,12,14] that its low-temperature asymptotic behavior is described by $N(E=0,T) \sim T^{d-1}$. However, some simulations[15] have found a stronger temperature dependence, i.e., $N(E=0,T) \sim T^{\lambda}$ with $\lambda > (d-1)$. For $d=2$, Sarvestani et al.[15] found $\lambda=1.75\pm0.1$, and for $d=3$, $\lambda=2.7\pm0.1$.

In Figure 11 we show our results in a log-log plot of $N(E=0,T)$ for various values of σ at $L=8$. At low temperatures the curves are quite straight on a log-log plot. So we can fit the low-temperature part of these curves to a power law form $N(E=0,T) \sim T^{\lambda}$. The fits are shown as solid lines in Fig. 11 and in Fig. 12. We plot λ as a function of σ in Fig. 13. We find that λ varies between 3 to 16 and is always greater than $d-1=2$ since $d=3$. Even in the case of uniform disorder (uniform random), $\lambda=4.8$. The large value of λ for $\sigma=0$ is not entirely surprising since Figure 10 shows that $N(E=0,T)$ is larger for $\sigma=0$ than for any other value of the disorder in the vicinity of the transition temperature. Since $N(E=0,T)$ goes to zero as the temperature goes to zero, $N(E=0,T)$ has the farthest to go for $\sigma=0$. Even though T_C is largest for $\sigma=0$, the ratio $N(E=0,T)/T_C$ is largest for the case of no disorder, and so it is consistent that the exponent λ is largest for the case of no disorder.
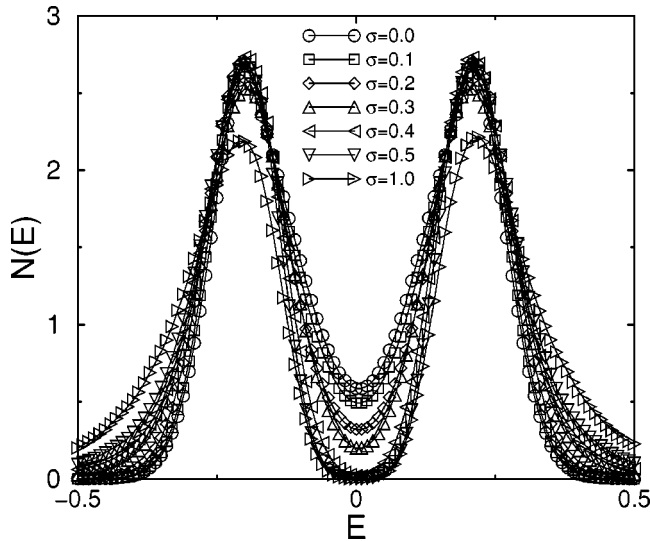
FIG. 10. $N(E)$ vs E for $L=8$ for various values of σ at temperatures in the vicinity of T_C. Shown are $\sigma=0$ ($T=0.128$, 45 runs), $\sigma=0.1$ ($T=0.122$, 10 runs), $\sigma=0.2$ ($T=0.105$, 5 runs), $\sigma=0.3$ ($T=0.085$, 15 runs), $\sigma=0.4$ ($T=0.045$, 115 runs), $\sigma=0.5$ ($T=0.030$, 45 runs), and $\sigma=1$ ($T=0.0275$, 108 runs). The temperatures and the number of runs averaged over are indicated in parentheses. The solid lines are guides to the eye.

We plot the data from Fig. 11 on a linear plot in Fig. 14 where we see S-shaped curves. We can see that $N(E=0,T)$ rises much more steeply for small values of disorder than for large values of disorder. The steepest part of the rise for the ordered cases ($\sigma \leq 0.3$) occurs approximately at T_C. We can quantify this by taking a derivative $dN(E=0)/dT$ that can be approximated by a finite difference:

$$\left. \frac{dN(E=0)}{dT} \right|_{T=T_i} \approx \frac{N_{i+1}(E=0) - N_i(E=0)}{T_{i+1} - T_i}. \quad (21)$$
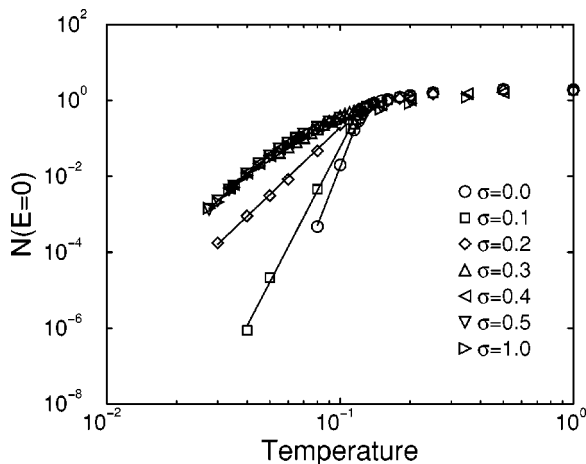
FIG. 11. Log-log plot of $N(E=0)$ versus T for $L=8$ for $\sigma=0$ (45 runs), $\sigma=0.1$ (15 runs), $\sigma=0.2$ (10 runs), $\sigma=0.3$ (10 runs), $\sigma=0.4$ (115 runs), $\sigma=0.5$ (45 runs), and $\sigma=1$ (108 runs). The number of runs averaged over is indicated in parentheses. The solid lines are power law fits to the data at low temperatures.
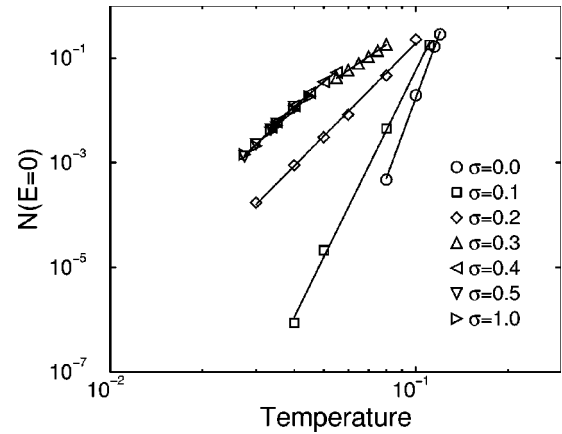

FIG. 12. Log-log plot of $N(E=0)$ vs T at low temperature for $L=8$ for $\sigma=0$ (45 runs), $\sigma=0.1$ (15 runs), $\sigma=0.2$ (10 runs), $\sigma=0.3$ (10 runs), $\sigma=0.4$ (115 runs), $\sigma=0.5$ (45 runs), and $\sigma=1$ (108 runs). The number of runs averaged over is indicated in parentheses. The solid lines are power law fits to the form $N(E=0,T) \sim T^\lambda$.

The result is shown in Fig. 6 where we compare T_C with the temperature T_{max} where $dN(E=0)/dT$ is a maximum. We see that T_{max} follows T_C for $\sigma \leq 0.3$ but lies above T_C for larger values of the disorder σ.

Efros and Shklovskiĭ[9,10] argued that at $T=0$ the Coulomb gap in the single-particle density of states of a fully disordered system should scale as $N(E) \sim |E-E_F|^\delta$, where $\delta=d-1$ and d is the dimension of the system. Some subsequent work[11,14,35] has supported this form for the density of states, though some simulations[5,12,15,51] have found a steeper energy dependence, i.e., $d > \delta > (d-1)$ in two[5,12,15,51] and three[12,15,51] dimensions. Efros[52] included two-electron transitions in calculating the density of states of a Coulomb glass and proposed the exponential form $N(E) \sim \exp[-|E_0/(E-E_F)|^{1/2}]$ where E_0 is a constant. The physical reason for such a sharp gap is the formation of polarons in which an occupied site tends to have unoccupied sites nearby and vice versa. Some simulations[5] have found support for this exponential form, while others[35,51] have not.

According to the theory,[9,10] $N(E) \sim |E-E_F|^{d-1}$ in the limit $E \to E_F$. In Fig. 15 we plot our data for $[N(E)-N(E_F)]$ versus
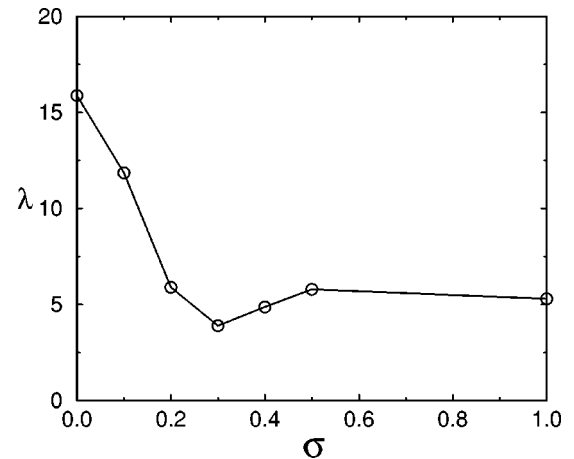

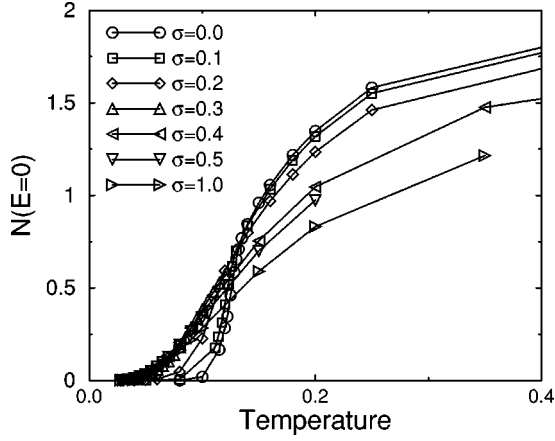FIG. 13. The power λ vs σ for $L=8$. The solid line is a guide to the eye.

FIG. 14. Linear plot of $N(E=0)$ vs T for $L=8$. Data are the same as shown in Fig. 11. The solid lines are guides to the eye.

FIG. 16. The exponent δ vs σ from the fits to the power law $[N(E)-N(0)]\sim|E-E_F|^\delta$ in Fig. 15. The solid line is a guide to the eye. The error in δ is approximately ±0.2 due to finite-size and finite-temperature effects described in the text.

$|E-E_F|$ on a log-log plot. [Since we are at finite temperatures, we have subtracted off $N(E_F)$.] We fit the low-energy data in the vicinity of the Fermi energy E_F to a power law of the form $N(E)\sim|E-E_F|^\delta$ for various values of σ at temperatures below T_C. For the case of strong disorder ($\sigma=1$), we find $\delta=2.65\pm0.2$, which agrees with the previous values of $\delta=2.6\pm0.2$ found by Möbius et al.[51] and $\delta=2.7\pm0.1$ found by Sarvestani et al.[15] It disagrees with the value of $\delta=d-1=2$ predicted by Efros and Shklovskii[9,10] and with the value $\delta=2.38$ found by Li and Phillips.[12] In the case of no disorder, the curvature is very close to quadratic and we find $\delta=2.1\pm0.2$. In Fig. 16 we plot the exponent δ versus the disorder σ. We see that δ increases and then saturates with increasing disorder. The estimated error of ±0.2 in δ does not come from the fit to the data, so much as from the fact that the finite temperature affects low energies $E\lesssim kT$. There are also finite size effects[51] that affect low energies $E\lesssim1/2L$,

though finite-size effects for $L\geq6$ are quite small (less than 1%).

We have checked to see if our data provide evidence for the exponential form $N(E)\sim\exp[-|E_0/(E-E_F)|^{1/2}]$ proposed by Efros.[52] In Fig. 17 we show a log-log plot of $-1/\ln[N(E)-N(E_F)]$ versus $|E-E_F|$ for various values of σ. [Since we are at finite temperatures, we have subtracted off $N(E_F)$.] If $N(E)\sim\exp[-|E_0/(E-E_F)|^{1/2}]$ were a good description of the density of states, then the curves in Fig. 17 would be straight lines with slopes of $1/2$. Since the exponential form presumably only describes the density of states in the vicinity of E_F, we have fit lines through the points corresponding to $|E|<0.04$ assuming the more general form $[N(E)-N(E_F)]\sim\exp-|E_0/(E-E_F)|^\gamma$. The slope of the lines in Fig. 17 correspond to the exponent γ. We plot γ versus σ
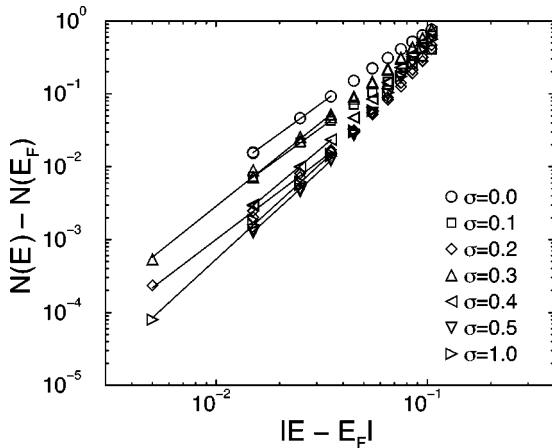

FIG. 15. Log-log plot of $[N(E)-N(E_F)]$ vs $|E-E_F|$ for $L=8$ for $\sigma=0$ ($T=0.120$, 45 runs), $\sigma=0.1$ ($T=0.111$, 15 runs), $\sigma=0.2$ ($T=0.08$, 20 runs), $\sigma=0.3$ ($T=0.055$, 15 runs), $\sigma=0.4$ ($T=0.0335$, 115 runs), $\sigma=0.5$ ($T=0.0275$, 45 runs), $\sigma=1.0$ ($T=0.0300$, 108 runs). The temperatues are all below T_C. The solid lines are fits to a power law $[N(E)-N(0)]\sim|E-E_F|^\delta$ for values of E very close to the Fermi energy E_F, i.e., $|E-E_F|<0.04$. The plots include $N(E)$ values for E above and below E_F.
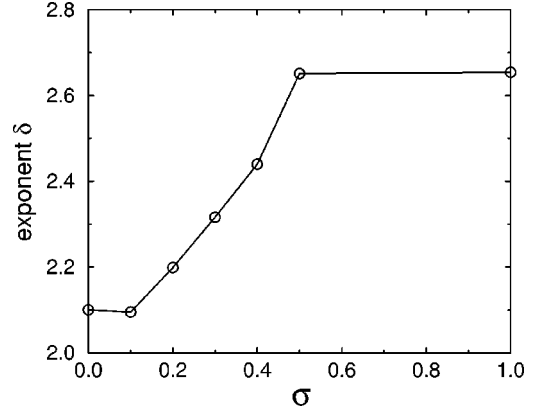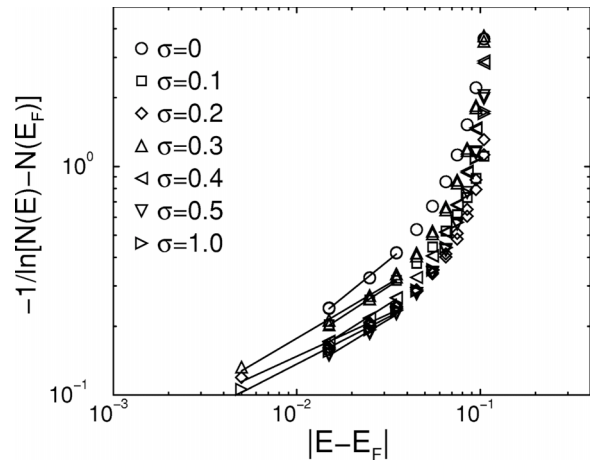

FIG. 17. Log-log plot of $-1/\ln[N(E)-N(E_F)]$ vs $|E-E_F|$ for $L=8$ for $\sigma=0$ ($T=0.120$, 45 runs), $\sigma=0.1$ ($T=0.111$, 15 runs), $\sigma=0.2$ ($T=0.08$, 20 runs), $\sigma=0.3$ ($T=0.055$, 15 runs), $\sigma=0.4$ ($T=0.0335$, 115 runs), $\sigma=0.5$ ($T=0.0275$, 45 runs), $\sigma=1.0$ ($T=0.0300$, 108 runs). The temperatues are all below T_C. The solid lines are fits to $-1/\ln[N(E)-N(E_F)]\sim|E-E_F|^\gamma$ for values of E very close to the Fermi energy E_F, i.e., $|E-E_F|<0.04$. The slope of each line gives γ. The plots include $N(E)$ values for E above and below E_F.
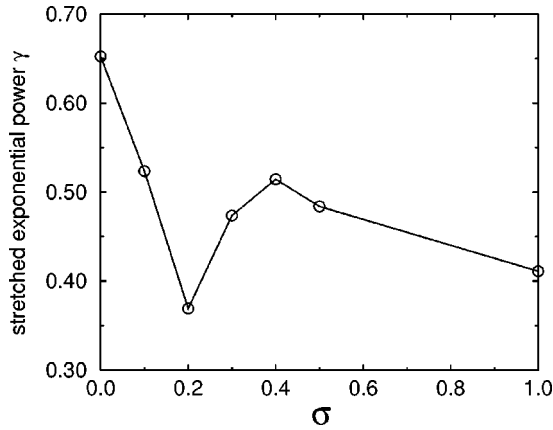
FIG. 18. The exponent γ vs σ from the fits to the exponential form $[N(E)-N(E_F)] \sim \exp|-E_0/(E-E_F)|^{\gamma}$ in Fig. 17. The solid line is a guide to the eye.

in Fig. 18. The values of γ fluctuate around $1/2$, but the large curvature of the trajectories in Fig. 17 do not lend strong support to the exponential form of the density of states.

Analytical theories[13,14] of the Coulomb glass predict that the finite-temperature density of states $N(E=0,T)$ at the Fermi energy ($E_F=0$) should be proportional to the zero-temperature density of states $N(E,T=0)$ at an energy $E=k_B T$, i.e., $N(E=0,T) \sim N(E,T=0)$ with $|E-E_F|=k_B T$. This has been supported by Coulomb glass simulations.[15] We tested this relation by plotting $N(E=0,T)$ versus T, and $N(E,T=T_0)$ versus E on the same graph, where T_0 is the lowest temperature at which we were able to equilibrate the system. We show our results in Fig. 19 for $\sigma=0$ and 1. The hypothesis seems to work for a limited range of energies between $k_B T_0$ and the width of the Coulomb gap. It also appears to be more applicable for high disorder ($\sigma=1$) than for the case of no disorder ($\sigma=0$).

E. Staggered occupation

We have studied the staggered occupation at various values of the disorder. At high temperatures the distribution has a peak centered at $M_s=0$ for all values of the disorder. At low temperatures the distribution broadens and has two peaks symmetrically placed about zero for the ordered case and for small and moderate values of the disorder. For the strongly disordered case $\sigma \geq 0.5$, the distribution has a peak centered at $M_s=0$ for all values of the temperature where the system was able to attain equilibrium in our simulations. This is what one would expect for a random system. These features are illustrated in Fig. 20, which shows the staggered occupation for various values of σ in the vicinity of T_C. As a function of system size, the high-temperature peak in $P(M_s)$ becomes sharper as L increases for all values of σ. An example is shown in Fig. 21.

V. SUMMARY

We have performed a Monte Carlo study of a classical three-dimensional Coulomb system of electrons in which we
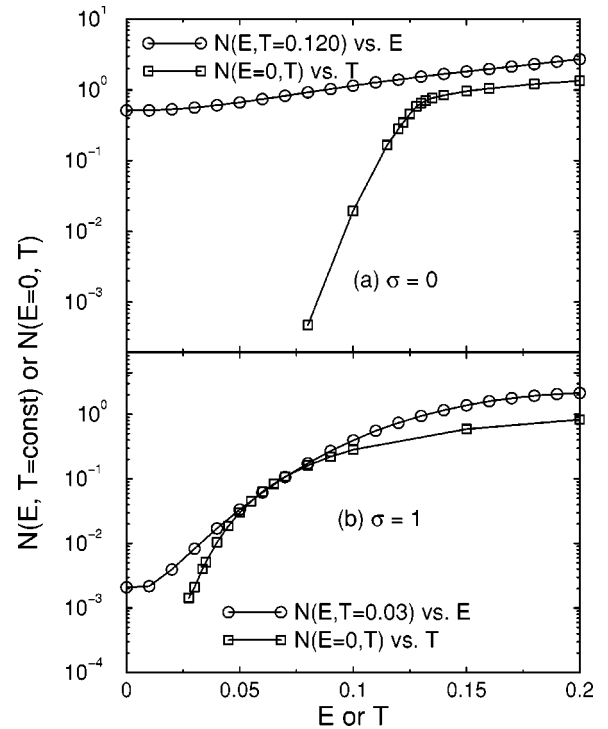

FIG. 19. (a) $N(E=0,T)$ vs T, and $N(E,T=0.120)$ vs E for $\sigma=0$. The data are averaged over 45 runs. (b) $N(E=0,T)$ vs T, and $N(E,T=0.0275)$ vs E for $\sigma=1$. The data are averaged over 108 runs. The solid lines are guides to the eye.

systematically increase the positional disorder by introducing deviations from positions in a cubic lattice. We start from a completely ordered system and gradually transition to a Coulomb glass. The phase transition as a function of temperature is second order for all values of disorder. We use finite-size scaling to determine the transition temperature T_C and the critical exponent ν. We find that T_C decreases and that ν increases with increasing disorder. Both quantities saturate in
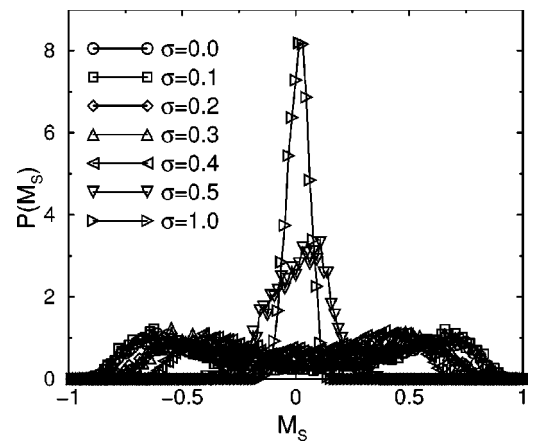

FIG. 20. Staggered occupation distribution for $L=8$ for various values of σ in the vicinity of T_C. $\sigma=0$ (35 runs, $T=0.128$), $\sigma=0.1$ (15 runs, $T=0.123$), $\sigma=0.2$ (10 runs, $T=0.110$), $\sigma=0.3$ (10 runs, $T=0.085$), $\sigma=0.4$ (40 runs, $T=0.045$), $\sigma=0.5$ (10 runs, $T=0.03$), and $\sigma=1$ (10 runs, $T=0.03$). The number of runs averaged over is indicated in parentheses. The solid lines are guides to the eye.
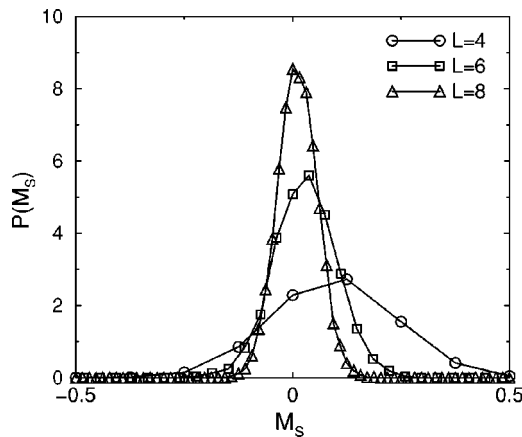
FIG. 21. Staggered occupation distribution for $\sigma=1$ at $T=1$ for $L=4$, 6, and 8. The peak height increases with increasing L. The data shown are the result of averaging over 10 runs. The solid lines are guides to the eye.

the limit of large disorder. The specific heat peak value decreases and the peak broadens to a broad bump with increasing disorder. A gap develops in the single-particle density of states for all values of σ. At low temperatures $N(E=0)\sim T^{\lambda}$ where $\lambda > 3.8$ for all values of σ. At low temperatures and low energies near E_F, the density of states can be fitted to a power law form $N(E)\sim|E-E_F|^{\delta}$ where $d-1<\delta<d$ for all values of σ. δ increases with increasing σ, starting at $\delta=2.1$ for $\sigma=0$ and saturating at $\delta=2.65$ for $\sigma=1$. The distribution of the staggered occupation has a single central peak at high temperature for all values of the disorder. In the ordered cases ($\sigma\lesssim0.4$) $P(M_s)$ develops two peaks symmetrically placed on either side of $M_s=0$ in the vicinity of the phase transition.

[1] A. Möbius and P. Thomas, Phys. Rev. B **55**, 7460 (1997).

[2] A. Möbius, P. Thomas, J. Talamantes, and C. J. Adkins, Philos. Mag. B **81**, 1105 (2001).

[3] E. R. Grannan and C. C. Yu, Phys. Rev. Lett. **71**, 3335 (1993).

[4] J. H. Davies, P. A. Lee, and T. M. Rice, Phys. Rev. Lett. **49**, 758 (1982).

[5] J. H. Davies, P. A. Lee, and T. M. Rice, Phys. Rev. B **29**, 4260 (1984).

[6] M. Grünewald, B. Pohlmann, L. Schweitzer, and D. Wurtz, J. Phys. C **15**, L1153 (1982).

[7] T. Vojta, J. Phys. A **26**, 2883 (1993).

[8] M. Pollak, Discuss. Faraday Soc. **50**, 13 (1970).

[9] A. L. Efros and B. I. Shklovskiĭ, J. Phys. C **8** L49 (1975).

[10] B. I. Shklovskiĭ and A. L. Efros, *Electronic Properties of Doped Semiconductors* (Spinger-Verlag, Berlin, 1984).

[11] E. I. Levin, V. L. Nguyen, B. I. Shklovskiĭ, and A. L. Éfros, Zh. Eksp. Teor. Fiz. **92**, 1499 (1987) [Sov. Phys. JETP **65**, 842 (1987)].

[12] Q. Li and P. Phillips, Phys. Rev. B **49**, 10 269 (1994).

[13] A. A. Mogilyanskiĭ and M. E. Raĭkh, Zh. Eksp. Teor. Fiz. **95**, 1870 (1989) [Sov. Phys. JETP **68**, 1081 (1989)].

[14] T. Vojta, W. John, and M. Schreiber, J. Phys.: Condens. Matter **5**, 4989 (1993).

[15] M. Sarvestani, M. Schreiber, and T. Vojta, Phys. Rev. B **52**, R3820 (1995).

[16] J. G. Massey and M. Lee, Phys. Rev. Lett. **75**, 4266 (1995).

[17] J. G. Massey and M. Lee, Phys. Rev. Lett. **77**, 3399 (1996).

[18] M. Lee, J. G. Massey, V. L. Nguyen, and B. I. Shklovskii, Phys. Rev. B **60**, 1582 (1999).

[19] B. Sandow *et al.*, Phys. Rev. Lett. **86**, 1845 (2001).

[20] A. Ciach and G. Stell, Physica A **306**, 220 (2002), and references therein.

[21] A. Z. Panagiotopoulos and S. K. Kumar, Phys. Rev. Lett. **83**, 2981 (1999).

[22] R. Dickman and G. Stell, in *Simulation and Theory of Electrostatic Interactions in Solutions*, edited by L. R. Pratt and G. Hummer (AIP, Woodbury, NY, 1999), p. 225.

[23] A. Brognara, A. Parola, and L. Reatto, Phys. Rev. E **65**, 066113 (2002), and references therein.

[24] M. E. Fisher, S. K. Ma, and B. G. Nickel, Phys. Rev. Lett. **29**, 917 (1972).

[25] E. Luijten and H. W. J. Blöte, Phys. Rev. Lett. **89**, 025703 (2002).

[26] H. G. Katzgraber and A. P. Young, Phys. Rev. B **67**, 134410 (2003).

[27] H. G. Katzgraber and A. P. Young, Phys. Rev. B **68**, 224408 (2003).

[28] A. J. Bray and M. A. Moore, J. Phys. C **17** L463 (1984).

[29] W. L. McMillan, Phys. Rev. B **29**, 4026 (1984).

[30] W. L. McMillan, Phys. Rev. B **30**, 476 (1984).

[31] H. Rieger *et al.*, J. Phys. A **29**, 3939 (1996).

[32] A. K. Hartmann and A. P. Young, Phys. Rev. B **64**, 180404 (2001).

[33] A. C. Carter, A. J. Bray, and M. A. Moore, Phys. Rev. Lett. **88**, 077201 (2002).

[34] D. S. Fisher and D. A. Huse, Phys. Rev. B **38**, 386 (1988).

[35] S. D. Baranovskiĭ, A. L. Efros, B. L. Gel'mont, and B. I. Shklovskiĭ, J. Phys. C **12**, 1023 (1979).

[36] A. Díaz-Sánchez *et al.*, Phys. Rev. B **62**, 8030 (2000).

[37] T. Vojta and M. Schreiber, Phys. Rev. Lett. **73**, 2933 (1994).

[38] E. R. Grannan and C. C. Yu, Phys. Rev. Lett. **73**, 2934 (1994).

[39] A. Möbius (private communication).

[40] A. Möbius and U. K. Rößler, cond-mat/0309001 (unpublished).

[41] W. Xue and P. A. Lee, Phys. Rev. B **38**, 9093 (1988).

[42] S. W. de Leeuw, J. W. Perram, and E. R. Smith, Proc. R. Soc. London, Ser. A **373**, 27 (1980).

[43] R. N. Bhatt and A. P. Young, Phys. Rev. B **37**, 5606 (1988).

[44] K. Binder, Z. Phys. B: Condens. Matter **43**, 119 (1981).

[45] A. Ciach (private communication).

[46] K. Vollmayr, J. D. Reger, M. Scheucher, and K. Binder, Z. Phys. B: Condens. Matter **91**, 113 (1993).

[47] A. P. Young (private communications).

[48] M. E. Fisher, J. Stat. Phys. **75**, 1 (1994).

[49] E. Luijten, M. E. Fisher, and A. Z. Panagiotopoulos, Phys. Rev. Lett. **88**, 185701 (2002).

[50] K. Binder and A. P. Young, Rev. Mod. Phys. **58**, 801 (1986).

[51] A. Möbius, M. Richter, and B. Drittler, Phys. Rev. B **45**, 11 568 (1992).

[52] A. L. Efros, J. Phys. C **9**, 2021 (1976).